ARTICLES

Neutral strange particle production in neutrino and antineutrino charged-current interactions on neon

D. DeProspo,[16*] M. Kalelkar,[16] M. Aderholz,[13] H. Akbari,[19†] P.P. Allport,[15] V.V. Ammosov,[9] A. Andryakov,[11] A. Asratyan,[11] S.K. Badyal,[12] H.C. Ballagh,[1] J.-P. Baton,[17] M. Barth,[3] H.H. Bingham,[1] E.B. Brucker,[18] R.A. Burnstein,[10] R.J. Cence,[7] T.K. Chatterjee,[5] E.F. Clayton,[8] G. Corrigan,[15] C. Coutures,[17] Devanand,[12] E. De Wolf,[3] P. Ermolov,[14] I. Erofeeva,[14] P.J.W. Faulkner,[2] H. Foeth,[4] W.B. Fretter,[1‡] G. Gapienko,[9] V.K. Gupta,[12] J. Hanlon,[6] G. Harigel,[4] F.A. Harris,[7] A. Ivanilov,[9] M. Jabiol,[17] P. Jacques,[16] V. Jain,[7§] G.T. Jones,[2] M.D. Jones,[7] T. Kafka,[19] V. Kaftanov,[11] P. Kasper,[17] V. Kobrin,[14] J.M. Kohli,[5] E.L. Koller,[18] V. Korablev,[9] M. Kubantsev,[11] M. Lauko,[16] O. Lukina,[14] J.E. Lys,[1] S. Lyutov,[14] P. Marage,[3] R.H. Milburn,[19] I.S. Mittra,[5] M.M. Mobayyen,[8] J. Moreels,[3] D.R.O. Morrison,[4] V. Moskalev,[11] V. Murzin,[14] G. Myatt,[15] P. Nailor[8] R. Naon,[10] A. Napier,[19] M. Neveu,[17] D. Passmore,[19] M.W. Peters,[7] V.Z. Peterson,[7] R. Plano,[16] N.K. Rao,[12] H.A. Rubin,[10] S. Ryasakov,[14] J. Sacton,[3] S.S. Sambyal,[12] N. Schmitz,[13] J. Schneps,[19] J.B. Singh,[5] S. Singh,[5] S. Sivoklokov,[14] W. Smart,[6] L. Smirnova,[14] P. Stamer,[16‖] K.E. Varvell,[2] L. Verluyten,[3] H. Wachsmuth,[4] S. Wainstein,[8] S. Willocq,[19¶] and G.P. Yost[1]

(E632 Collaboration)

[1] *University of California, Berkeley, California 94720*
[2] *University of Birmingham, Birmingham B15 2TT, United Kingdom*
[3] *Inter-University Institute for High Energies (Université Libre de Bruxelles–Vrije Universiteit te Brussels), B-1050 Brussels, Belgium*
[4] *CERN, CH-1211 Geneva 23, Switzerland*
[5] *Panjab University, Chandigarh 160014, India*
[6] *Fermilab, Batavia, Illinois 60510*
[7] *University of Hawaii, Honolulu, Hawaii 96822*
[8] *Imperial College, London SW7 2AZ, United Kingdom*
[9] *Institute of High Energy Physics, Serpukhov, 142284 Protvino Moscow region, Russia*
[10] *Illinois Institute of Technology, Chicago, Illinois 60616*
[11] *Institute of Theoretical and Experimental Physics, 117259 Moscow, Russia*
[12] *University of Jammu, Jammu 180001, India*
[13] *Max-Planck-Institut fur Physik, D-80805 Munich, Germany*
[14] *Moscow State University, 177234 Moscow, Russia*
[15] *Oxford University, Oxford OX1 3RH, United Kingdom*
[16] *Rutgers University, New Brunswick, New Jersey 08903*
[17] *Centre d'Etudes Nucleaires de Saclay, F-91191 Gif-sur-Yvette CEDEX, France*
[18] *Stevens Institute of Technology, Hoboken, New Jersey 07030*
[19] *Tufts University, Medford, Massachusetts 02155*

(Received 31 May 1994)

A study has been made of neutral strange particle production in $\nu_\mu Ne$ and $\bar{\nu}_\mu Ne$ charged-current interactions at a higher energy than any previous study. The experiment was done at the Fermilab Tevatron using the 15-ft. bubble chamber, and the data sample consists of 814(154) observed neutral strange particles from 6263(1115) $\nu(\bar{\nu})$ charged-current events. For the ν beam (average event energy $\langle E_\nu \rangle = 150$ GeV), the average multiplicities per charged-current event have been measured to be 0.408 ± 0.048 for K^0, 0.127 ± 0.014 for Λ, and 0.015 ± 0.005 for $\bar{\Lambda}$, which are significantly greater than for lower-energy experiments. The dependence of rates on kinematical variables has been measured, and shows that both K^0 and Λ production increase strongly with E_ν, W^2, Q^2, and y_B. Compared to lower-energy experiments, single-particle distributions indicate that there is much more K^0 production for $x_F > -0.2$, and the enhanced Λ production spans most of the kinematic region. $\bar{\Lambda}$ production is mostly in the region $|x_F| < 0.3$. The Lund model is shown to be in qualitative agreement with the data, but does not reproduce single-particle distributions in

*Present address: Arete Engineering Technologies Corp., P.O. Box 16407, Arlington, VA 22215.
†Present address: CERN, CH-1211 Geneva 23, Switzerland.
‡Deceased.
§Present address: Wilson Lab., Cornell Univ., Ithaca, NY 14853.
‖Permanent address: Seton Hall Univ., S. Orange, NJ 07079.
¶Present address: SLAC Bin 96, P.O. Box 4349, Stanford, CA 94309.

detail. For $x_F > -0.2$ there is a significant excess of Λ production over the model's prediction. The Λ hyperons are found to be polarized in the production plane.

PACS number(s): 13.15.+g, 14.20.Jn, 14.40.Aq

I. INTRODUCTION

There have been a number of published results [1–16] on neutral strange particle production in charged-current (CC) ν_μ and $\bar{\nu}_\mu$ interactions. It has been realized that the dominant mechanism is associated production of $s\bar{s}$ quark pairs during hadronization. However, another significant source is Cabibbo-favored decays of c or $\bar{c}$ quarks. In $\nu(\bar{\nu})$ interactions, $c(\bar{c})$ quarks can be produced directly from the strange sea or via Cabibbo-suppressed production on $d(\bar{d})$ quarks. Finally, in $\bar{\nu}$ interactions it is possible to have Cabibbo-suppressed single s-quark production from a valence u quark. These processes account for virtually all of the strange particle production, although a few other possible mechanisms do exist, involving Cabibbo-suppressed $s(\bar{s})$ production from $u(\bar{u})$ quarks in the sea.

In all of these processes the strange hadrons in the final state may be charged or neutral. A notable advantage of studying neutral strange particles is that they can be cleanly identified by kinematic fitting, so that backgrounds are negligible and do not bias the measurements significantly. It is noteworthy that all such investigations, including our own, have come from bubble chamber experiments. No other technique has so far yielded results on strange particle production by neutrinos.

Most of the previous experiments have been at average neutrino event energies of about 50 GeV. Typically these experiments have found that both the K^0 and Λ multiplicities increase with neutrino energy, the K^0 much more so than the Λ multiplicity. They have also found that the K^0's are produced mostly in the central rapidity region, while the Λ's come from target fragmentation.

We have done a study of neutral strange particle production in an experiment (E632) at the Fermilab Tevatron featuring higher neutrino energies than any previous work. The average energy of ν_μ CC events was 150 GeV, while that for $\bar{\nu}_\mu$ was 110 GeV. We have examined the effect of higher energies not only on neutral strange particle multiplicities, but on production mechanisms as well. Comparisons with previous lower-energy experiments have revealed significant differences in multiplicities as well as in production characteristics.

II. EXPERIMENTAL PROCEDURE

The data for this experiment (E632) were acquired in two runs at the Fermilab Tevatron. The neutrino beam was produced by the quadrupole triplet train (tuned to a momentum of 300 GeV/c), which focused secondary particles produced by the interactions of 800 GeV protons from the Tevatron. The sample reported here corresponds to 1.66×10^{17} protons on target. The secondaries entered a 532-m tunnel, and the beam of neutrinos originated from the decays of charged mesons in this tunnel. At the end of the tunnel was a 1-km earth shield containing a primary dirt fill followed by iron, lead, and concrete. The primary fill absorbed hadrons, while the rest of the shield stopped all but a few of the muons. Neutrinos passed through the shield into the detector.

The detector was the 15-ft. bubble chamber filled with a liquid neon-hydrogen mixture which also served as the target. A fiducial volume of about 15 m^3 in the first run (10 m^3 in the second run) was employed, in which ν and $\bar{\nu}$ CC events were produced in a ratio of 6 to 1, with mean energies of 150 GeV and 110 GeV, respectively. The chamber was in a magnetic field of 3 T.

The chamber liquid consisted of 75% molar neon in the first run (63% in the second run) with a density of 0.71 g/cm^3 (0.54 g/cm^3). The interaction length for hadrons in this liquid was 125 cm (165 cm), so that hadrons typically interacted within the chamber, whereas muons left the chamber without interacting. The photon conversion length was 42 cm (55 cm) so that most γ's from neutral pion decay underwent pair production in the chamber.

Photographs of the chamber made by three cameras were examined, and events on film were selected for measurement. For some of the rolls of film, all events were measured, while for the rest of the rolls only those events were measured that included possible neutral strange particle decays (called vees). All tracks from the primary vertex were measured, as well as associated vees and γ conversions. All tracks were geometrically reconstructed.

The bubble chamber was equipped with arrays of proportional tubes: an internal picket fence (IPF) to determine the event time, and an external muon identifier (EMI) to identify muons. Muon candidates were required to have a momentum exceeding 5 GeV/c, to leave the chamber without interacting, and to have a good two-plane match in the EMI, corresponding to traversal through 7 to 11 hadronic interaction lengths after the bubble chamber. Approximately 96% of muons above 5 GeV/c were within the EMI acceptance, and the identification efficiency for them was about 95%, with little background ($< 0.7\%$) from hadron punchthrough, meson decays, or accidental association. For details about the EMI, see Refs. [17–19].

The charged-current sample was defined as those events having a muon identified by the above criteria, and a total hadronic effective mass greater than 2 GeV. (See Sec. IV for details on how the hadronic effective mass was calculated.) If there was more than one muon candidate in an event, the one with the largest momentum component transverse to the neutrino direction was taken to be the CC-defining muon.

Kinematic fitting of all measured vees and γ's was attempted. The following hypotheses were tried as constrained fits to the production vertex: $K_S \to \pi^+\pi^-$, $\Lambda \to p\pi^-$, $\bar{\Lambda} \to \bar{p}\pi^+$, and $\gamma + N \to (N)e^+e^-$. To select the vee candidates, constrained fits were required to have a probability greater than 0.1%. (If a vee made fits to additional origins besides the production vertex, the latter was selected if its probability exceeded 1%, or if it had

the highest probability.) This resulted in 995 vee candidates, of which about half came from rolls of film on which all CC events had been measured. The other half were from rolls on which only events with vees were measured, so as to obtain an enriched vee sample. Since the flux of protons on target was known for every roll, it was possible to derive the number of CC events even on those rolls on which only events with vees were measured. The data reported in this paper correspond to 6263 ± 110 ν and 1115 ± 46 $\bar{\nu}$ CC events.

Of the 995 vee candidates, 37 or about 4% were ambiguous between strange particle and the γ hypothesis. These were taken to be γ's if the unconstrained effective mass of the decay tracks, when interpreted as e^+e^-, was less than 70 MeV. As a result, 27 vee candidates were reclassified as γ's, leaving a sample of 968 vees, of which 814 were from ν CC events, and 154 from $\bar{\nu}$ CC events.

About 20% of the vees had acceptable fits for both the K_S and Λ hypotheses, and another 8% were $K_S/\bar{\Lambda}$ ambiguities. (There were no Λ-$\bar{\Lambda}$ ambiguities, but two vees were triply ambiguous.) To resolve ambiguities, the probabilities $P(K_S)$, $P(\Lambda)$, and $P(\bar{\Lambda})$ for the competing fits were compared. To be selected as a $\bar{\Lambda}$, it was required that $P(\bar{\Lambda}) > P(\Lambda)$, and $P(\bar{\Lambda}) > P(K_S) + 0.3$. If these conditions were not satisfied, the vee was selected as a K_S if $P(K_S) > P(\Lambda) + 0.1$, and the remaining ambiguities were assigned to the Λ sample. This algorithm for resolving ambiguities was devised in order to produce an isotropic K_S decay angular distribution, which is the distribution of the cosine of the angle between the K_S line of flight and the direction of the decay π^+ in the K_S rest frame. This is a suitable algorithm to use, since the K_S is spinless and therefore must have an isotropic decay angular distribution. It was found that 29% of the K_S/Λ ambiguities were resolved as K_S, while 89% of the $K_S/\bar{\Lambda}$ were resolved as K_S.

Figure 1 shows the decay angular distributions for K_S and Λ after resolution of ambiguities. The distribution is indeed isotropic for the K_S sample. The distribution for Λ is roughly isotropic, but there is some departure from isotropy near $\cos\theta \sim 1$. That region corresponds to decay π^+ mesons with low momentum in the laboratory, which makes such Λ's difficult to find and to reconstruct. A correction for this depletion must be made when calculating rates, as will be described in the next section. It may be noted that we do not have a similar loss due to low-momentum decay protons, because protons carry a much larger fraction of the Λ momentum than do pions. For our Λ sample, the median momentum of the decay protons is about 1.7 GeV/c, while that of decay pions is only 0.34 GeV/c.

Table I gives the numbers of observed K_S, Λ, and $\bar{\Lambda}$ from ν and $\bar{\nu}$ CC interactions after resolution of ambiguities. To select the final vee sample for physics analysis, two cuts were made. Vee vertices were required to be at least 1 cm from the primary vertex, because the decay tracks of closer vees can be confused with charged tracks emanating from the primary vertex. Also, vee vertices were required to be at least 20 cm in front of the chamber wall in order to provide adequate decay track length for momentum measurement. Fewer than 8% of the vees were eliminated by these cuts, and Table I gives the remaining numbers of K_S, Λ, and $\bar{\Lambda}$ in the final sample. About 22% of the K_S in the final sample were from ambiguous fits, as were 42% of the Λ and 30% of the $\bar{\Lambda}$.

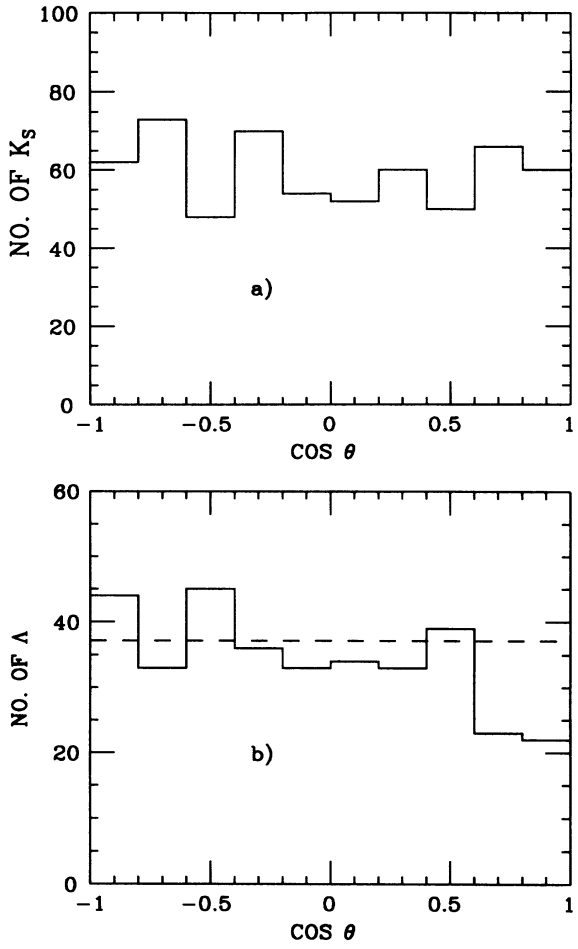

FIG. 1. Decay angular distributions for (a) K_S and (b) Λ. These are distributions of the cosine of the angle between the vee line of flight and the direction of the positive decay product in the vee rest frame. The dashed line was used to estimate the loss in the depleted bins.

Figure 2 shows the unconstrained invariant mass distributions for the decay tracks from K_S and Λ. Also shown are the results of fits to the distributions using Gaussian shapes. These fits yielded mass values of 497.9 ± 0.9 MeV for the K_S, and 1115.7 ± 0.4 MeV for the Λ, which are both in excellent agreement with the world-average values [20]. The Gaussian fits also yielded a standard

TABLE I. Observed numbers of neutral strange particles from ν and $\bar{\nu}$ charged-current (CC) events, before and after cuts.

	K_S	Λ	$\bar{\Lambda}$
From 6263 ν CC events, before cuts	502	285	27
From 6263 ν CC events, after cuts	470	258	24
From 1115 $\bar{\nu}$ CC events, before cuts	93	57	4
From 1115 $\bar{\nu}$ CC events, after cuts	88	51	3

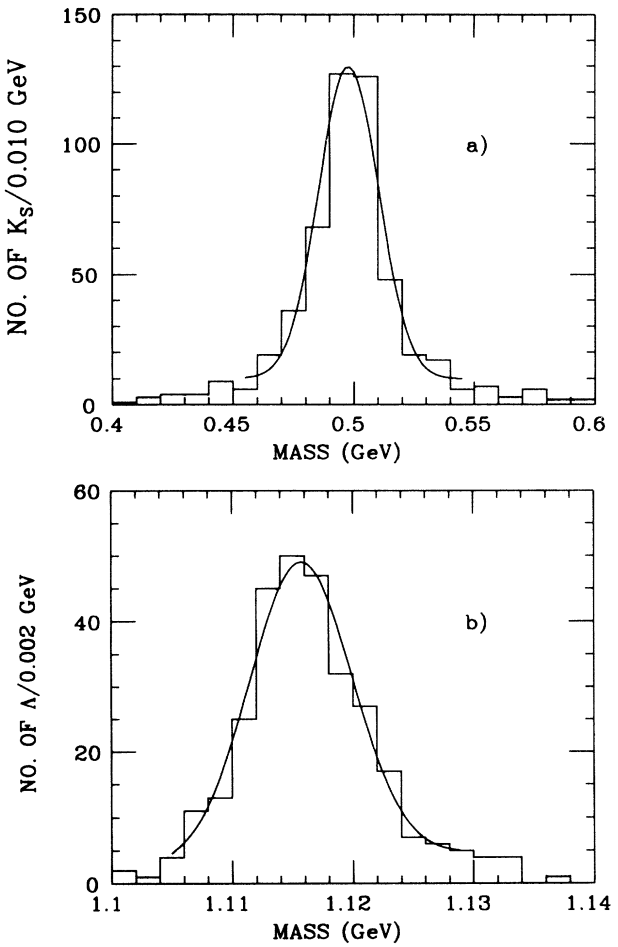

FIG. 2. Unconstrained invariant-mass distributions of (a) $\pi^+\pi^-$ from decays of K_S in the final sample, and (b) $p\pi^-$ from decays of Λ in the final sample. The curves represent Gaussian fits as described in the text.

deviation $\sigma = 12$ MeV for the K_S, and 4.2 MeV for the Λ, which are indications of our experimental mass resolutions in the K_S and Λ regions.

Although Table I gives the total numbers of observed vees in the final sample, it is also of interest to consider how often there are multiple vees in an event. Table II gives the numbers of ν and $\bar{\nu}$ CC events with each possible combination of observed vees.

TABLE II. Numbers of charged-current events with a specified combination of observed neutral strange particle decays. X indicates any hadron system not containing observed K_S, Λ, or $\bar{\Lambda}$.

	ν CC events	$\bar{\nu}$ CC events
$K_S X$	364	73
ΛX	208	41
$\bar{\Lambda} X$	17	3
$K_S K_S X$	27	3
$K_S \Lambda X$	35	7
$K_S \bar{\Lambda} X$	3	0
$\Lambda\Lambda X$	3	1
$\Lambda\bar{\Lambda} X$	4	0
$K_S K_S K_S X$	2	0
$K_S K_S \Lambda X$	2	1
$K_S \Lambda\Lambda X$	1	0
$K_S K_S K_S \Lambda X$	1	0

III. PRODUCTION RATES

To obtain inclusive production rates, the observed numbers of vees were corrected for various sources of loss. These are explained below, and the average value of each weight for each type of vee is given in Table III.

(a) The geometric detection efficiency, which is momentum dependent, was calculated separately for each vee by using the minimum length cut of 1.0 cm and a maximum potential length which was the distance, along the particular vee's line of flight, from the primary vertex to a point 20 cm in front of the chamber wall.

(b) Each vee was weighted for the probability of decay before interaction within the length of liquid that it actually traversed.

(c) Vees were weighted both for scanning and fitting efficiency as well as for systematic losses of the energetic vees which can get obscured by the forward cone of charged tracks from the primary vertex. Random scanning losses were calculated by performing a second scan on some rolls of film, and comparing the results with the first scan. To estimate systematic losses, a careful, dedicated scan was made on about 25% of the sample by a physicist who checked especially for vees hidden among other tracks, and vees far from the primary vertex. This dedicated scan revealed that vees with energy greater than 20 GeV had lower efficiencies for being found in a routine scan than vees of lesser energy. Such high energy vees were therefore given an extra weight, whose effect was to increase the overall scanning weight by 5% for K_S and $\bar{\Lambda}$, but only 1% for Λ, because Λ's are generally of lower energy (see Sec. IV).

(d) The proper decay length for each K_S was calculated from the length in the laboratory as measured beyond the initial 1.0 cm minimum length cut. In the distribution of the proper decay length there was a depletion for $c\tau < 1.5$ cm. An exponential fit to the distribution in the region $c\tau > 1.5$ cm yielded a mean proper decay length of 2.3 ± 0.3 cm, with a χ^2 of 4.3 for 7 degrees of freedom, consistent with the known value [20] of 2.675 cm. Then the fit was extrapolated to $c\tau = 0$, and the low-lifetime loss was calculated by comparing the expected number of K_S with the observed number below $c\tau = 1.5$ cm. The correction for K_S was 1.03 ± 0.02, and the same procedure for Λ's and $\bar{\Lambda}$'s gave a weight of 1.06 ± 0.02. (The mean proper decay length for Λ's was 7.5 ± 1.4 cm, with a χ^2 of 5.2 for 11 degrees of freedom, consistent with the known value of 7.89 cm.)

(e) Λ's were corrected for the anisotropy in the decay angular distribution mentioned in the previous section (see Fig. 1). For $\cos\theta > 0.6$ there is some loss because of the difficulty of finding and reconstructing Λ's with low-momentum decay pions, which characterize that kinematic region. The distribution for $\cos\theta < 0.6$ was extrapolated into the region $\cos\theta > 0.6$ to determine the loss in the depleted bins, which required a weight of 1.06 ± 0.02. To check whether this correction is reasonable, we have

TABLE III. Average weights applied to observed neutral strange particles.

	K_S	Λ	$\bar{\Lambda}$
Geometric detection	1.18 ± 0.01	1.16 ± 0.01	1.25 ± 0.06
Decay before interaction	1.23 ± 0.01	1.20 ± 0.02	1.50 ± 0.09
Scanning and/or reconstruction losses	1.16 ± 0.08	1.13 ± 0.07	1.18 ± 0.10
Low-lifetime loss	1.03 ± 0.02	1.06 ± 0.02	1.06 ± 0.02
Low-momentum π^-		1.06 ± 0.02	
Ambiguity resolution	1.00 ± 0.04	1.00 ± 0.04	1.00 ± 0.20

examined the momentum distribution of our decay pions, and find that 75 MeV/c is approximately the lowest momentum that we reconstruct. For Λ's with the actual observed momentum distribution, a straightforward calculation (assuming an isotropic decay) shows that most of the observed anisotropy is accounted for by the loss of decay pions below 75 MeV/c. We do not have a loss corresponding to low-momentum decay protons, because the calculation for our Λ's indicates that there would be no protons below about 150 MeV/c, and we have found that we can construct protons down to that value. Finally, we have checked that for our K_S and $\bar{\Lambda}$ with their actual momentum distribution, a negligible fraction would have a decay pion below 75 MeV/c, so no correction is needed.

(f) As shown in the previous section, the algorithm for resolving ambiguities is statistically valid for the sample as a whole. To determine the uncertainty in the ambiguity resolution procedure, an estimate was made of how many vees could be differently assigned while still maintaining consistency with isotropy in the decay angular distribution for the spinless K_S.

After applying all these corrections, the average experimental weights were 1.86 ± 0.20 for K_S, 1.97 ± 0.18 for Λ, and 2.57 ± 0.67 for $\bar{\Lambda}$. (Because of correlations, these overall weights are slightly greater than the products of the corresponding weights in Table III.) An additional weight for decay branching ratios was then applied (including the factor of 2 for K_L), and Table IV gives the fully corrected average multiplicities per CC event. (For the rest of this paper, all references to K^0 really mean $K^0 + \bar{K}^0$.) For ν_μ CC events, the mean multiplicities are 0.408 ± 0.048 for K^0, 0.127 ± 0.014 for Λ, and 0.015 ± 0.005 for $\bar{\Lambda}$. The quoted errors include statistical errors as well as the uncertainties in calculating each of the correction factors, and the uncertainty in the ambiguity resolution algorithm. The ratio of Λ to K^0 production is 0.31 ± 0.05 for ν, and 0.26 ± 0.06 for $\bar{\nu}$.

Table V compares our measurements of the K^0 and Λ production rates with the most statistically significant previous results. It should be noted that all of the previous experiments have been at much lower energies than ours. Although those experiments have used a variety of targets and event selection criteria, they exhibit a general consistency in the K^0 and Λ rates, especially in the former. By contrast, our measurements of these rates give significantly higher values. In the next section we explore whether our higher rates can be attributed to the higher neutrino energies, and whether the K^0 and Λ production properties are different from those at lower energies.

We have made use of the γ conversions to search for Σ^0 hyperon production. Figure 3 shows the $\Lambda\gamma$ effective mass distribution for ν CC events, and reveals a small signal at the Σ^0 mass. To determine the production rate, we have fitted the distribution to a polynomial background plus a Gaussian shape for the Σ^0, fixing only the mass. This yielded an estimate of 15 Σ^0 above background, and $\sigma = (6 \pm 3)$ MeV for the Gaussian. We then tried another method of evaluating the background. We calculated a $\Lambda\gamma$ effective mass distribution using Λ's and γ's from different events but with similar values of total hadronic invariant mass. This background distribution was normalized to the true distribution excluding the Σ^0 region (1.16–1.22 GeV). Using this normalized background yielded an estimate of 14 true Σ^0, which is close to the estimate using the Gaussian fit. However, it may be noted in Fig. 3 that in the bin immediately following the Σ^0 signal, there is a depletion that is comparable in magnitude to the Σ^0 signal. Accordingly the

TABLE IV. Average neutral strange particle multiplicities per charged-current (CC) event. The K^0 rate includes $K^0 + \bar{K}^0$. The Λ rate includes Λ's from Σ^0 decay.

	K_S	Λ	$\bar{\Lambda}$
ν CC events	0.408 ± 0.048	0.127 ± 0.014	0.015 ± 0.005
$\bar{\nu}$ CC events	0.454 ± 0.078	0.118 ± 0.019	0.010 ± 0.007

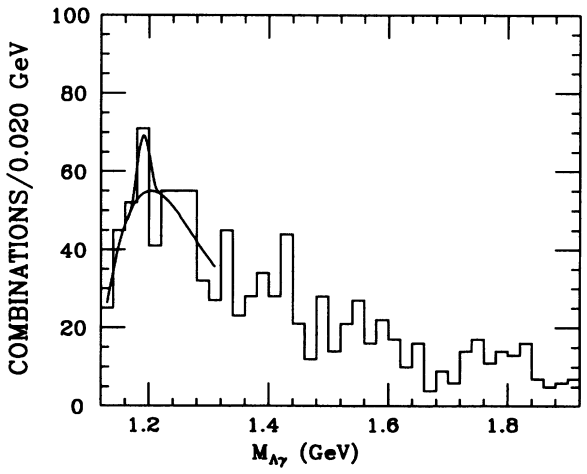

FIG. 3. Effective mass distribution for $\Lambda\gamma$ combinations using fitted Λ and γ from ν charged-current events. The solid lines represent the results of a fit to the distribution using a Gaussian shape for the Σ hyperon and a polynomial for the background.

TABLE V. Inclusive production rates for K^0 and Λ per charged-current event. N_K and N_Λ are the observed numbers of K_S and Λ, respectively, while the rates are fully corrected. K^0 includes $K^0 + \bar{K}^0$.

Reaction [Ref.]	$\langle E_\nu \rangle$ (GeV)	N_K	K^0 Rate (%)	N_Λ	Λ Rate (%)
ν-Ne [This expt.]	150	502	40.8 ± 4.8	285	12.7 ± 1.4
ν-Ne [10]	103	203	23.0 ± 1.7	98	5.7 ± 0.7
ν-n [12]	~ 60		20.5 ± 1.2		6.6 ± 0.7
ν-p [12]	~ 60		17.4 ± 1.2		4.4 ± 0.5
ν-p [16]	51	831	19.0 ± 0.9	491	5.2 ± 0.3
ν-Ne [14]	46	2279	16.8 ± 1.2	1843	6.5 ± 0.5
ν-p [9]	43	359	17.5 ± 0.9	180	4.5 ± 0.4
$\bar{\nu}$-Ne [This expt.]	110	93	45.4 ± 7.8	57	11.8 ± 1.9
$\bar{\nu}$-Ne [10]	81	64	21.9 ± 2.8	37	6.5 ± 1.2
$\bar{\nu}$-Ne [6]	~ 45	350	16.4 ± 0.9	257	6.3 ± 0.4
$\bar{\nu}$-p [8]	~ 45	88	15.1 ± 3.2	46	4.5 ± 0.9
$\bar{\nu}$-n [12]	~ 45		20.8 ± 2.0		7.6 ± 0.8
$\bar{\nu}$-p [12]	~ 45		18.4 ± 1.3		5.7 ± 0.6
$\bar{\nu}$-Ne [15]	40	518	15.7 ± 0.8	469	8.2 ± 0.5
$\bar{\nu}$-p [16]	40	401	16.1 ± 0.9	344	5.7 ± 0.4

Σ^0 signal cannot be regarded as decisive, and a large uncertainty is unavoidable. We have used an estimate of 15 ± 8 Σ^0 events. This observed rate was corrected for Λ detection efficiencies (discussed above) as well as the γ detection and reconstruction efficiency of $(42 \pm 4)\%$. We finally obtained a total inclusive Σ^0 production rate of $(1.8 \pm 1.1)\%$ as a fraction of all neutrino charged-current events, where the error includes the uncertainties in estimating the small signal and in calculating all the detection efficiencies. For comparison, a previous ν experiment [14] and a $\bar{\nu}$ experiment [15] measured rates of $(1.1 \pm 0.3)\%$ and $(0.6 \pm 0.3)\%$, respectively. Both of these experiments had mean neutrino energies of about 45 GeV compared to 150 GeV for ours. From our production rate, we derive the fraction of Λ's coming from Σ^0 decay to be $(14 \pm 8)\%$, which is very similar to that of Ref. [14].

IV. PRODUCTION PROPERTIES

To investigate neutral strange particle production mechanisms, we have measured the average K^0 and Λ multiplicities as functions of (a) E_ν, the neutrino energy, (b) $Q^2 = 2E_\nu(E_\mu - P_\mu^L) - m_\mu^2$, the invariant square of the four-momentum transfer from the neutrino to the muon, where the muon energy E_μ and longitudinal momentum P_μ^L are in the laboratory frame, (c) $W^2 = 2m_p(E_\nu - E_\mu) + m_p^2 - Q^2$, the invariant square of the hadronic system's effective mass, (d) $x_B = Q^2/2m_p(E_\nu - E_\mu)$, the Bjorken scaling variable, and (e) $y_B = (E_\nu - E_\mu)/E_\nu$, the fractional energy transfer to the hadronic system. All results presented in this section will be for the ν events only, because our $\bar{\nu}$ events comprise only a small fraction of the total.

To determine the incident neutrino energy for each event, we have summed the energies of all charged tracks and associated neutrals. To correct for missing energy (mostly neutrals that do not materialize within the bubble chamber), we have employed the Bonn method [21], which is based partly on transverse momentum balance. The corrected neutrino energy is estimated to be given by $E_\nu = P_\mu^L + \Sigma P_h^L + (|P_\mu^T + \Sigma P_h^T|)\Sigma P_h^L / \Sigma |P_h^T|$, where P_h^L and P_h^T are the longitudinal and transverse momentum components, respectively, of a visible, measured particle. With this prescription the average correction to the hadronic energy is about 18%, and the resulting energy spectrum of events is in good agreement with a Monte Carlo calculation using the computed beam profile.

Figure 4 shows the average K^0 and Λ multiplicities as a function of incident neutrino energy. An unambiguous increase with energy is apparent, and the dashed lines in Fig. 4 show the results of linear fits to $\ln(N)$vs $\ln(E_\nu)$ for our data. The slopes of these fits are 0.48 ± 0.10 for the K^0, and 0.23 ± 0.11 for the Λ. We have also compared our data with the predictions of a Monte Carlo model based on the Lund model (JETSET 6.3), for which we have used the default value of 0.3 for the s/u quark ratio. Some previous neutrino experiments have found that a lower value of 0.2 for this ratio is needed to obtain reasonable agreement with their data. However, we note that the DELPHI experiment [22] at the CERN e^+e^- collider LEP has recently measured a value of 0.30 ± 0.02 which corroborates previous results from e^+e^- experiments at lower energies, and therefore we have retained the default. In fact we have used default values for all parameters except the diquark suppression $(us/ud)(d/s)$ which we have increased from 0.4 to 0.5 because the same experiment [23] has reported a value of 0.50 ± 0.06. The Monte Carlo calculation incorporates our actual neutrino beam energy spectrum and also includes detector resolution and efficiencies. The solid lines in Fig. 4 represent the predictions of the Lund model, and agree qualitatively with our data. For our neutrino spectrum, the model predicts overall multiplicities of 0.455, 0.111, and 0.017 for K^0, Λ, and $\bar{\Lambda}$, respectively, which are quite consistent with our measured values as given in Table IV. If we use the lower value $s/u = 0.2$, we obtain predicted multiplicities of 0.339 for K^0 and 0.082 for Λ, which are

much lower than our measured values. The higher energy of our experiment may be why our data prefer the higher value $s/u = 0.3$.

In Fig. 4 we also compare the energy dependence of our K^0 and Λ multiplicities with three previous experiments. For neutrino energies below 70 GeV, our K^0 rate is consistent with the older experiments. At higher energies the K^0 rate keeps increasing, which is the main reason why our overall rate is significantly higher than previous results. It should be noted, however, that the fit to our data (dashed line in Fig. 4) does lie above all of the points from other experiments. The same is true for the Λ. Note that one of the other experiments in the figure (Ref. [16]) used a hydrogen target, for which Λ production is expected to be smaller than for a neon target. A charged-current interaction on a valence d quark leaves a uu diquark in a proton but a ud diquark in a neutron. Additionally, secondary interactions can occur inside a neon nucleus or very close to the primary interaction point. A hadron experiment [24] has found that rescattering in the nucleus contributes significantly to enhancement of Λ production.

Production rates as functions of W^2, Q^2, x_B, and y_B are shown in Figs. 5–7. The K^0 rate increases clearly with W^2, Q^2, and y_B, but shows little or no dependence on x_B. Very similar observations have been made by previous experiments, although several have noted a falloff in the rate at the highest values of W^2 and y_B. They have attributed the apparent falloff to possible systematic losses of K^0 inside high-multiplicity jets and to smearing effects [14,15]. Our data do not show such an anomalous falloff; in our experiment, particular attention was paid to examining jets and showers for hidden vees. Our Λ rate also exhibits an increase with W^2, Q^2, and y_B, although the effect is less pronounced than for the K^0. The solid lines in Figs. 5–7 represent the predictions of the Lund model, which agree qualitatively with our data.

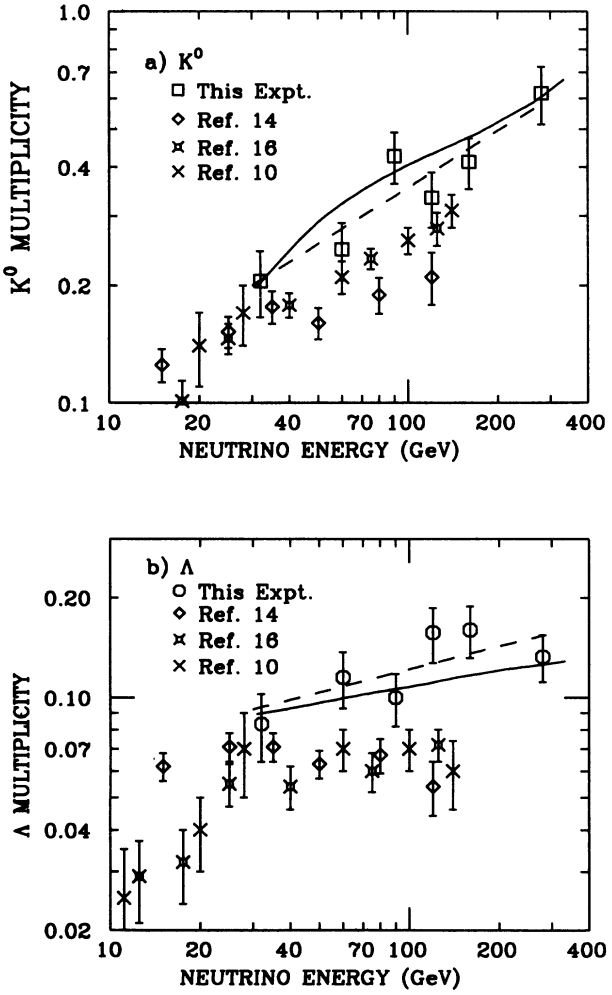

FIG. 4. Average multiplicity of (a) K^0 and (b) Λ as a function of the incident neutrino energy. These multiplicities are fully corrected for all sources of loss, and K^0 includes $K^0+\bar{K}^0$. The solid lines represent the predictions of the Lund Monte Carlo program, and the dashed lines represent linear fits to the data.

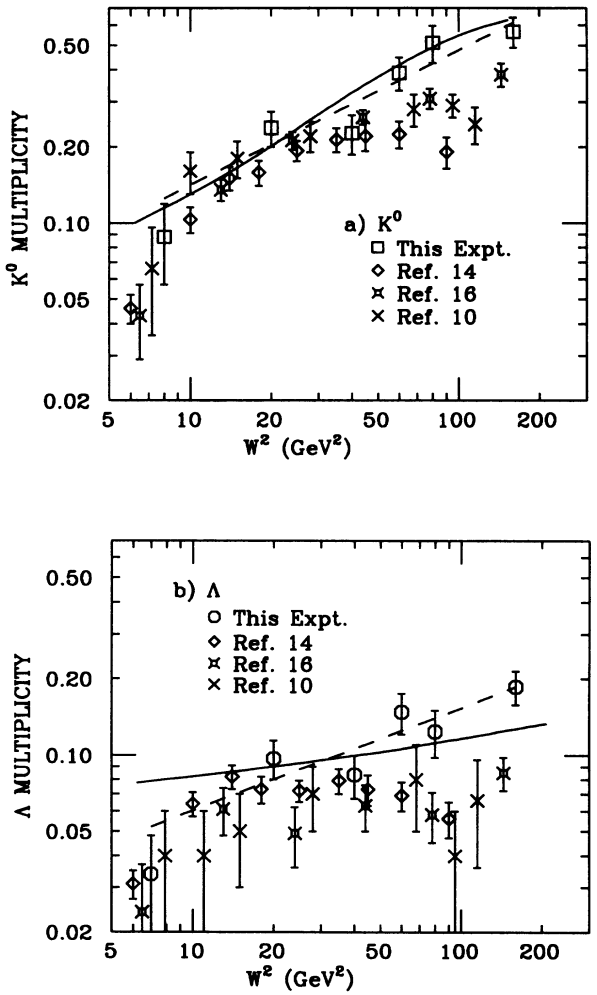

FIG. 5. Average multiplicity of (a) K^0 and (b) Λ as a function of W^2, the invariant square of the hadronic system's effective mass. The solid lines represent the predictions of the Lund Monte Carlo program, and the dashed lines represent linear fits to the data.

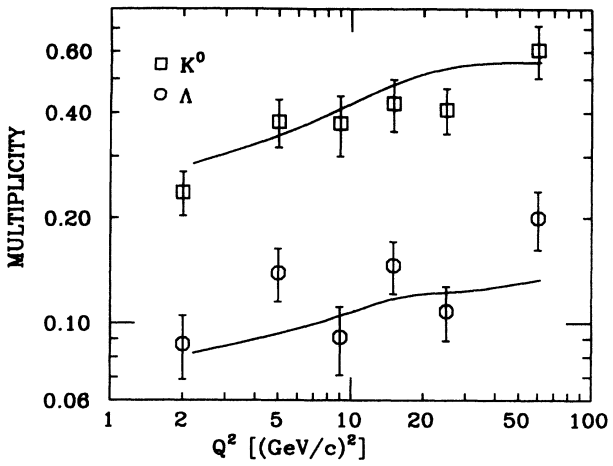

FIG. 6. Average K^0 and Λ multiplicities as a function of Q^2, the invariant square of the four-momentum transfer from the neutrino to the muon. The solid lines represent the predictions of the Lund Monte Carlo program.

The agreement is better for the K^0 than for the Λ.

The dashed lines in Fig. 5 show the results of linear fits to $\ln(N)$ vs $\ln(W^2)$. We obtain slopes of 0.53 ± 0.08 for the K^0, and 0.41 ± 0.09 for the Λ, and note that these are quite consistent with each other.

The differences in the production properties of K^0 and Λ are seen most clearly in single-particle distributions. In Fig. 8 we show the distributions of the Feynman-x variable $x_F = 2p_L^*/W$, where p_L^* is the longitudinal momentum of the particle in the hadronic center of mass. (The longitudinal direction is the hadronic system's direction of motion, and the hadronic system's four-vector was calculated using the muon and corrected neutrino four-momenta.) In Fig. 9 are shown the distributions of each particle's rapidity y^* in the hadronic center of mass, where $y^* = \frac{1}{2}\ln[(E^* + p_L^*)/(E^* - p_L^*)]$. In this expression, E^* is the particle's total energy in the hadronic center of mass. These are differential distributions, and are normalized to the total number of charged current events,

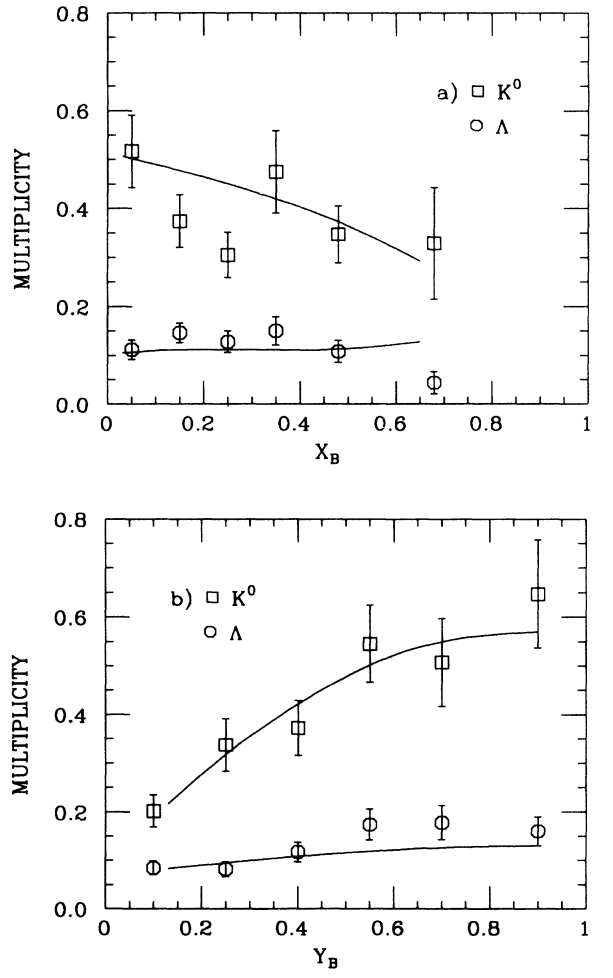

FIG. 7. Average K^0 and Λ multiplicities as functions of (a) the Bjorken scaling variable x_B, which is the fraction of the nucleon momentum carried by the struck quark, and (b) y_B, the fractional energy transfer to the hadron system. The solid lines represent the predictions of the Lund Monte Carlo program.

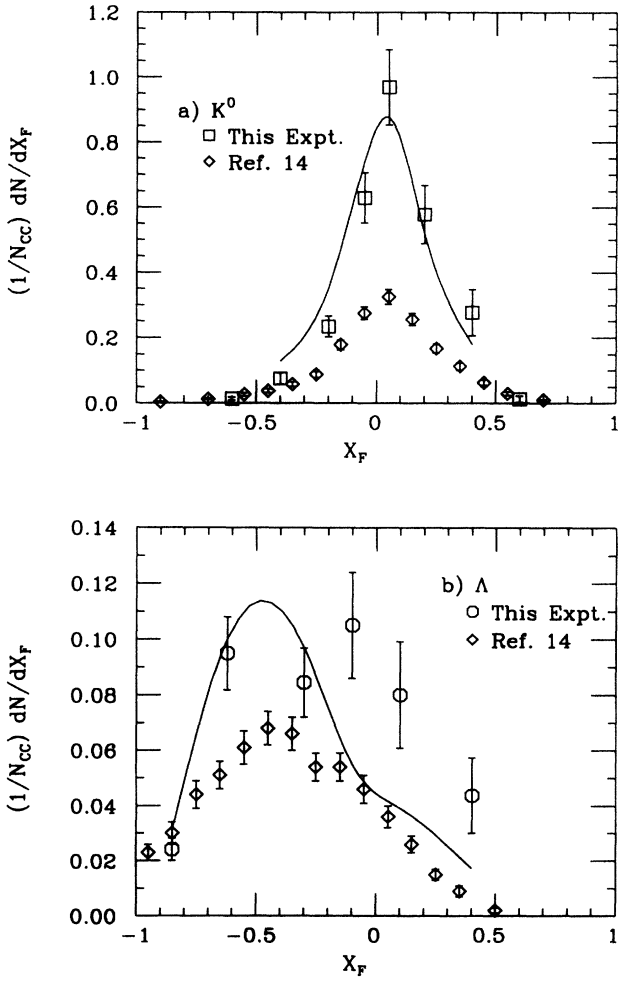

FIG. 8. Distributions of the Feynman-x variable for (a) K^0 and (b) Λ, normalized to the total number of charged-current events. The ordinate at any point represents the average multiplicity of the particle per unit interval of x_F. The solid lines represent the predictions of the Lund Monte Carlo program.

so that the ordinate at any point gives the average multiplicity of the particle per unit interval of the variable. Any misidentification of vees by the ambiguity resolution algorithm would mostly affect high values of x_F and y^*, as would the weight for systematic losses of high-energy vees. The error bars shown in the figures include the uncertainties due to these effects.

Figures 8 and 9 show that the Λ is produced mostly in the backward region, as expected from target fragmentation, but that there is non-negligible production in the central and forward regions as well. By contrast, the K^0 is produced mostly in the central region, with a significant excess in the forward region. In fact, we find that we have relatively more forward K^0 production than previous experiments, which were at lower energies. One way to illustrate this point is to consider the asymmetry parameter $A = (N_F - N_B)/(N_F + N_B)$, where N_F and N_B are the numbers of particles going forward and backward, respectively, in the hadronic center of mass. For the K^0, we measure $A = 0.35 \pm 0.04$ compared to 0.16 ± 0.02 that was reported by the previous experiment with the highest statistics [14]. That experiment had a much lower mean neutrino event energy of 46 GeV compared to 150 GeV for ours. For the Λ, we obtain $A = -0.47 \pm 0.07$ compared to -0.71 ± 0.02 for Ref. [14], showing the effect of much stronger forward Λ production. This energy dependence is confirmed in our own data: for events with $W^2 > 60$ GeV^2, the asymmetry parameter for K^0 is 0.40 ± 0.05 compared to 0.22 ± 0.08 for $W^2 < 60$ GeV^2. Similarly, the asymmetry parameters for Λ are -0.35 ± 0.09 and -0.69 ± 0.08 in those two regions. (We have checked that our results for the asymmetry are not very sensitive to the particular energy correction technique that we use. For example, in the extreme case where no correction is made at all, we measure for the full sample $A = 0.39 \pm 0.04$ for the K^0, and $A = -0.40 \pm 0.07$ for the Λ.)

Figures 8 and 9 include the Feynman-x and rapidity data from Ref. [14]. For the K^0, we have a large excess over Ref. [14], especially in the central and forward regions ($x_F > -0.2$, $y^* > -1$). For the Λ, our enhancement over Ref. [14] spans most of the kinematic region.

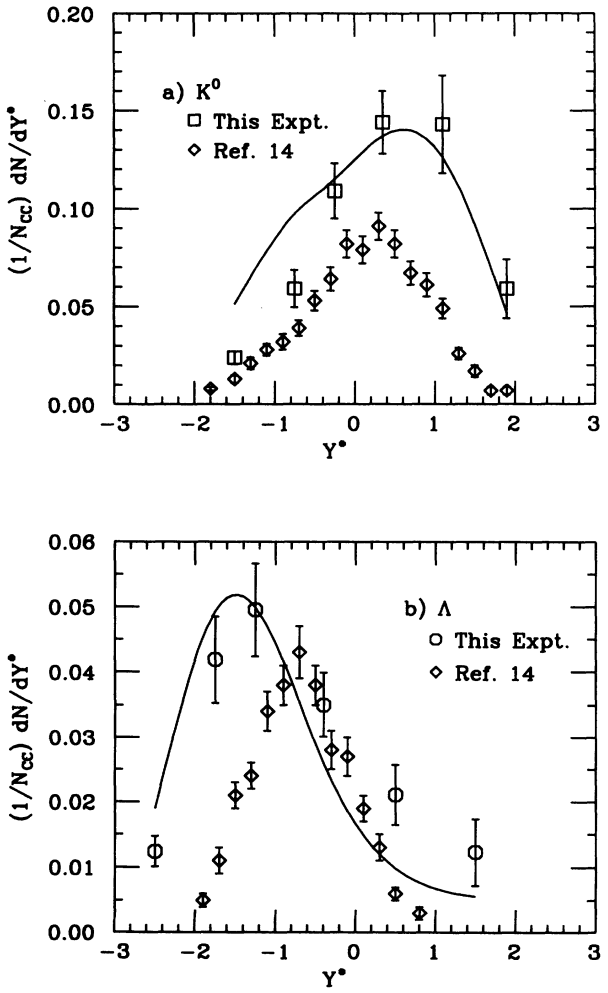

FIG. 9. Distributions of rapidity (in the hadronic system's center of mass) for (a) K^0 and (b) Λ, normalized to the total number of charged-current events. The solid lines represent the predictions of the Lund Monte Carlo program.

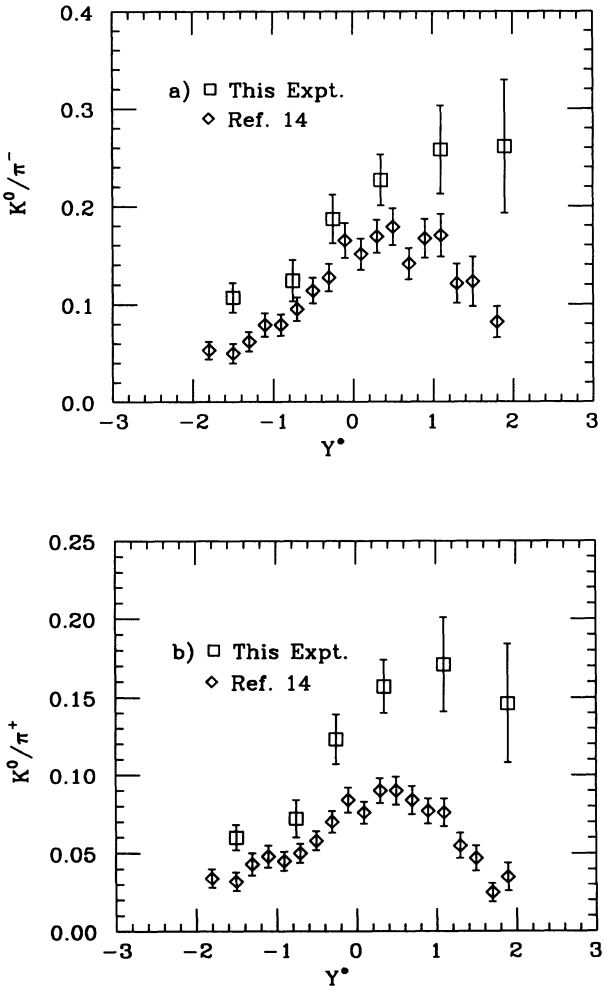

FIG. 10. Ratio of normalized center-of-mass rapidity distribution of K^0 to that of (a) π^- and (b) π^+ mesons produced in neutrino charged-current events.

The solid lines in Figs. 8 and 9 represent the predictions of the Lund model. Although the model is in qualitative agreement with our data, it does overestimate our K^0 rate for the backward region ($x_F < 0, y^* < 0$), and it underestimates our Λ rate for $x_F > -0.2, y^* > -1$. This disagreement is also reflected in the asymmetry parameter, which the Lund model predicts to be $+0.08$ and -0.71 for the K^0 and Λ, respectively.

It is instructive to compare the K^0 rapidity distribution with that of pions. In Fig. 10(a) we show the ratio of the normalized K^0 rapidity distribution to that for π^- mesons. There is a monotonic increase in the ratio as a function of rapidity, rising by a factor of two or three from the backward to the very forward region. Figure 10(b) shows the ratio of K^0 to π^+ mesons, and also exhibits a clear increase with rapidity. Data from Ref. [14] are included in Fig. 10 for comparison, and exhibit a similar rise with rapidity in the backward hemisphere, but are markedly different from our data in the forward hemisphere. We observe much stronger forward K^0 production than does Ref. [14].

In Fig. 11 we show the normalized distributions in p_T^2, the square of the momentum component transverse to the direction of motion of the hadronic system, and in z, the fraction of the total hadronic laboratory energy carried by the particle. As seen in the figure, the p_T^2 distributions are well described by a simple exponential. The dashed lines are the results of fits of the form $A\exp(-Bp_T^2)$. The fits yielded slope parameters of $B = 4.15 \pm 0.31$ $(\mathrm{GeV}/c)^{-2}$ for the K^0, and $B = 4.02 \pm 0.34$ $(\mathrm{GeV}/c)^{-2}$ for the Λ. These are very similar and are also consistent with values reported by previous experiments, although some of them [14,15] have found that above 0.5 $(\mathrm{GeV}/c)^2$ there is a possible change of slope. Within our statistics, we do not see any convincing evidence for a change of slope in our data.

Our z distributions are similar in shape to those seen in previous experiments at lower energies. Some of them, however, have reported a turnover at low z which may

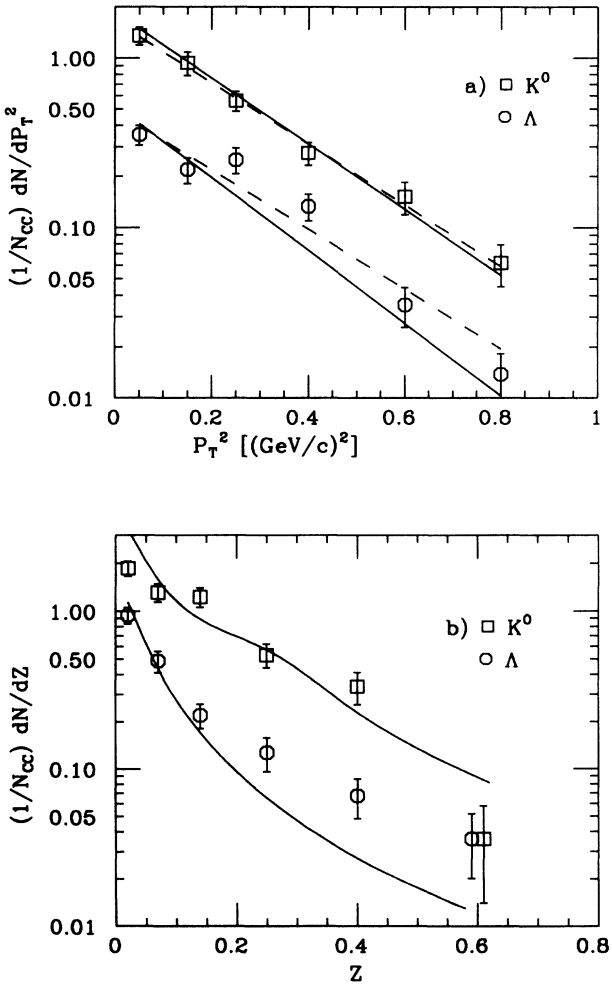

FIG. 11. Normalized differential distributions for K^0 and Λ of (a) p_T^2, the square of the momentum component transverse to the direction of motion of the hadronic system, and (b) z, the fraction of the total hadronic laboratory energy carried by the particle. The solid lines represent the predictions of the Lund Monte Carlo program, and the dashed lines represent the results of exponential fits described in the text.

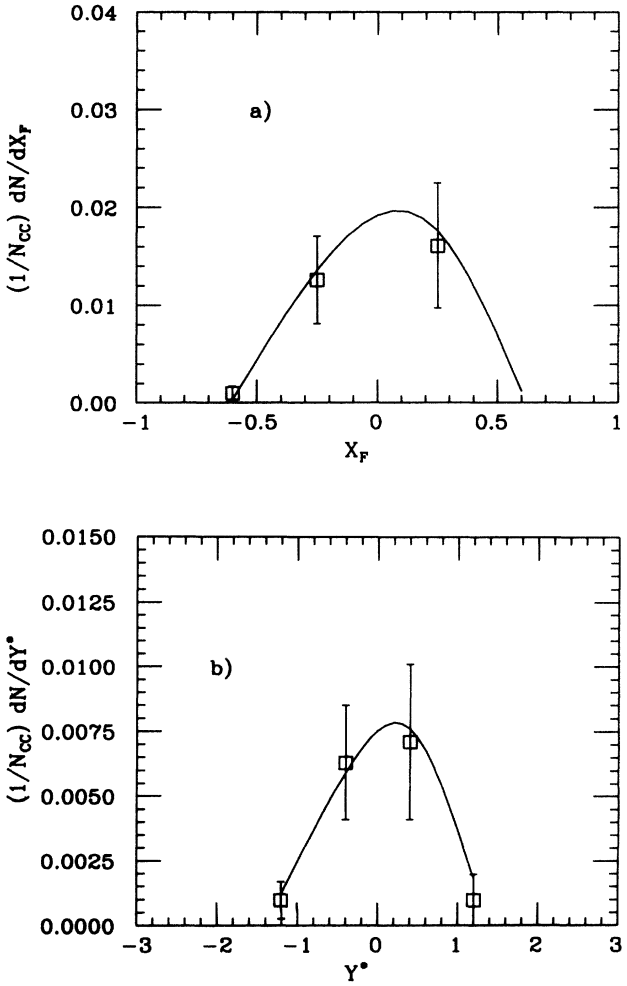

FIG. 12. Distributions of (a) Feynman-x and (b) center-of-mass rapidity for the $\bar{\Lambda}$, normalized to the total number of charged-current events. The solid lines represent the predictions of the Lund Monte Carlo program.

in part be due to rest mass effects. We do not observe a turnover, and it is noteworthy that the previous experiment with the highest energy [10] also did not observe a turnover. Rest mass effects are less important at higher energies. The solid lines in Fig. 11 represent the predictions of the Lund model.

Although our sample contains only a few $\bar{\Lambda}$ hyperons (see Table I), it is relatively clean, with only 30% of the $\bar{\Lambda}$ coming from ambiguous fits. Therefore we have attempted to extract some information on production properties, which previous experiments have not done. Figure 12 displays the normalized Feynman-x and rapidity distributions for the $\bar{\Lambda}$ hyperons. It is quite apparent that they are produced exclusively in the central region. The mean value of x_F for our $\bar{\Lambda}$ is -0.09 ± 0.07, and approximately 90% of them are contained within $|x_F| < 0.3$. Similarly, their mean value of y^* is -0.10 ± 0.13, and 90% of them are within $|y^*| < 1$. They are much more tightly bunched kinematically than the Λ. The forward-backward asymmetry for $\bar{\Lambda}$ is $A = 0.05 \pm 0.15$. Figure 12 also shows the predictions of the Lund model, which agrees remarkably well with our data.

V. Λ POLARIZATION

A theoretical analysis by Bigi [25] predicts that Λ polarization may be observed in neutrino interactions even though the target nucleon is unpolarized. The reason is that the W boson usually interacts with a left-handed valence d quark in the nucleon, leaving behind a polarized diquark which can eventually hadronize into a Λ. The Λ can inherit the polarization of the parent diquark. Two experiments [15,26] have emphasized the importance of selecting axes appropriately for polarization measurement. In the Λ rest frame, they have chosen the x axis to lie along the direction of the W boson, and they define the production plane to be the plane containing the directions of the W boson and the target nucleon. Then the y axis is perpendicular to the production plane, and the z axis is perpendicular to the W, but inside the production plane. With these definitions, both experiments concluded that there was no Λ polarization perpendicular to the production plane. Within the production plane, Ref. [15] observed clear evidence for polarization in the direction opposite to that of the W boson, i.e., in the negative x direction. Reference [26], on the other hand, found that kinematic cuts were necessary to obtain significant polarization, and it was not entirely opposite to the W direction. The results of these two experiments are summarized in Table VI. Two other experiments [5,11] have also measured Λ polarization, but have defined their axes differently and are therefore not directly comparable.

For our analysis using the ν CC sample, we have defined axes in the Λ rest frame as described above. If P is the polarization of the Λ along any of the axes, and θ is the angle of the decay proton relative to that axis, the fraction of Λ's as a function of θ is given by $\frac{df}{d(\cos\theta)} = \frac{1}{2}(1+\alpha P \cos\theta)$, where $\alpha = 0.642$ is the weak decay parameter [20] of the Λ. Figure 13 shows this angular distribution for the three axes, along with the results of linear fits. All of the fits were excellent with $\chi^2/N_{\rm DF} < 1$, and the polarizations that we derive are given in Table VI. In agreement with Refs. [15] and [26], we find no polarization perpendicular to the production plane. Within the plane, our results are intermediate between those of the previous experiments, with $P_x = -0.38 \pm 0.16$, a 2.4σ level of polarization in the direction opposite to that of the W boson. There is a possibility that the systematic loss of Λ's with low-momentum decay pions [see Fig. 1(b)] may introduce biases into the polarization plots, even though the axes are different. The largest effect might be expected on P_x because of partial correlation between the directions of the W and the Λ. By studying the effects of various kinematic cuts on the polarizations, we estimate that the systematic uncertainty on the polarizations may be comparable to the quoted statistical errors.

If Bigi's argument [25] is valid, it might be expected that polarization would be especially apparent for Λ's in the target fragmentation region. We have therefore repeated our analysis for Λ's with $x_F < 0$, and the results are given in Table VI along with those of the previous experiments. We do find that polarization in the production plane is modestly enhanced, and P_z becomes nonzero at the 2σ level in addition to P_x. Therefore our

TABLE VI. Λ Polarization. The x axis is along the W boson direction in the Λ rest frame. The other two axes are perpendicular to the W, with the y axis being transverse to the production plane, and the z axis inside the production plane.

Reaction [Ref.]	P_x	P_y	P_z
ν-Ne [This expt.]	-0.38 ± 0.16	-0.04 ± 0.17	-0.17 ± 0.18
$\bar{\nu}$-Ne [15]	-0.56 ± 0.13	-0.02 ± 0.13	0.08 ± 0.13
ν-p [26]	-0.10 ± 0.14	-0.02 ± 0.16	0.12 ± 0.15
$\bar{\nu}$-p [26]	-0.24 ± 0.17	-0.05 ± 0.16	-0.20 ± 0.17
ν-Ne, $x_F < 0$ [This expt.]	-0.43 ± 0.20	-0.06 ± 0.19	-0.45 ± 0.19
$\bar{\nu}$-Ne, $x_F < 0$ [15]	-0.63 ± 0.13	-0.02 ± 0.14	0.12 ± 0.14
ν-p, $x_F < 0$ [26]	-0.29 ± 0.18	-0.09 ± 0.19	0.19 ± 0.18
$\bar{\nu}$-p, $x_F < 0$ [26]	-0.38 ± 0.18	0.02 ± 0.18	-0.17 ± 0.18
K^0 control sample [This expt.]	-0.02 ± 0.08	0.10 ± 0.08	-0.10 ± 0.08

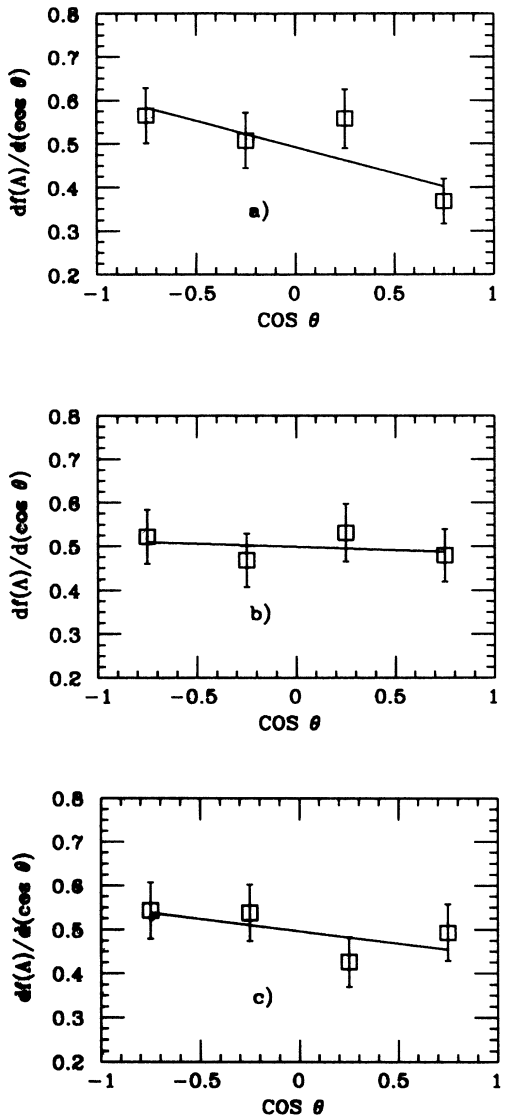

FIG. 13. Angular distributions of protons from Λ decay with respect to (a) the direction of the W boson in the Λ rest frame, (b) perpendicular to the W boson and to the production plane (defined by the W and the target nucleon), and (c) perpendicular to the W but within the production plane. The plots are normalized so that the integrals over the distributions are equal to one. The solid lines represent the results of linear fits.

measurements support Bigi's hypothesis that Λ polarization originates from a polarized diquark.

A useful control sample is provided by our K^0 mesons, which being spinless should not exhibit polarization along any direction. We have analyzed the K^0's by measuring the angular distribution of the decay π^+ and fitting exactly as for the Λ's. (Since there is no decay parameter for the K^0, we have set $\alpha = 1$.) Table VI gives the putative polarizations of K^0 along the three axes, all of which are consistent with zero.

We have also done one other systematic check to determine whether our results are sensitive to the neutrino energy correction technique (Bonn method) that we use. The directions of the axes do depend on the neutrino energy. However, even if we adopt the extreme case of making no correction at all to the neutrino energy, we obtain Λ polarizations of $P_x = -0.37 \pm 0.15$, $P_y = -0.04 \pm 0.16$, and $P_z = -0.22 \pm 0.17$, which are very similar to the values we derive when we do make the energy correction.

VI. SUMMARY

We have studied characteristics of neutral strange particle production in ν and $\bar{\nu}$ charged current interactions in the Fermilab 15-ft. bubble chamber filled with a heavy Ne-H_2 mix. The events have much higher energy ($\langle E \rangle = 150$ GeV) than in any previous such study. For the ν beam, we have measured inclusive production rates per event of $(40.8 \pm 4.8)\%$ for the K^0, $(12.7 \pm 1.4)\%$ for the Λ, and $(1.5 \pm 0.5)\%$ for the $\bar{\Lambda}$. These rates are considerably higher than those measured at lower energies. We have also measured a Σ^0 production rate of $(1.8 \pm 1.1)\%$, which corresponds to $(14 \pm 8)\%$ of Λ's coming from Σ^0 decay. For the $\bar{\nu}$ beam, production rates are $(45.4 \pm 7.8)\%$ for the K^0, $(11.8 \pm 1.9)\%$ for the Λ, and $(1.0 \pm 0.7)\%$ for the $\bar{\Lambda}$. The ratio of Λ to K^0 production is 0.31 ± 0.05 for ν, and 0.26 ± 0.06 for $\bar{\nu}$.

We have shown that both the K^0 and Λ production rates increase with E_ν, W^2, Q^2, and y_B, with the K^0 exhibiting an especially strong increase. No significant dependence on x_B is observed. Feynman-x and rapidity distributions show that the K^0 is mainly in the central region, but with significant production in the forward region. The Λ is mainly produced in the target fragmentation region, although there is appreciable central and forward production as well. Compared to lower-energy experiments, our K^0 production is enhanced in the region $x_F > -0.2$, while the Λ production is enhanced for essentially all x_F. The forward-backward asymmetry parameter is $+0.35 \pm 0.04$ for the K^0, and is -0.47 ± 0.07 for the Λ. The $\bar{\Lambda}$ are produced in a narrow region around $x_F = y^* = 0$, with an asymmetry parameter of $+0.05 \pm 0.15$. We have found that p_T^2 distributions for both K^0 and Λ can be described by simple exponentials with slopes that are consistent with each other. Most of these results are in qualitative agreement with the Lund model, though the single-particle distributions do not agree in detail. There is more Λ production for $x_F > -0.2$ than is predicted by the model.

Finally, we have measured a modest polarization of the Λ within the production plane, especially in the direction opposite to that of the W boson ($P_x = -0.38 \pm 0.16$). Perpendicular to the production plane the polarization is consistent with zero.

ACKNOWLEDGMENTS

We are grateful to the operating crews of the 15-ft. bubble chamber and the neutrino beam at Fermilab. We also thank the scanning and measuring staffs at our institutions. This work was supported in part by grants from the U.S. Department of Energy, the U.S. National Science Foundation, and the U.K. Science and Engineering Research Council.

[1] H. Deden *et al.*, Phys. Lett. **58B**, 361 (1975).
[2] J.P. Berge *et al.*, Phys. Rev. Lett. **36**, 127 (1976).
[3] J.P. Berge *et al.*, Phys. Rev. D **18**, 1359 (1978).
[4] O. Erriquez *et al.*, Nucl. Phys. **B140**, 123 (1978).
[5] V.V. Ammosov *et al.*, Nucl. Phys. **B162**, 205 (1980).
[6] V.V. Ammosov *et al.*, Nucl. Phys. **B177**, 365 (1981).
[7] N.J. Baker *et al.*, Phys. Rev. D **24**, 2779 (1981).
[8] R. Brock *et al.*, Phys. Rev. D **25**, 1753 (1982).
[9] H. Grassler *et al.*, Nucl. Phys. **B194**, 1 (1982).
[10] P. Bosetti *et al.*, Nucl. Phys. **B209**, 29 (1982).
[11] D. Allasia *et al.*, Nucl. Phys. **B224**, 1 (1983).
[12] D. Allasia *et al.*, Phys. Lett. **154B**, 231 (1985).
[13] V.V. Ammosov *et al.*, Z. Phys. C **30**, 183 (1986).
[14] N.J. Baker *et al.*, Phys. Rev. D **34**, 1251 (1986).
[15] S. Willocq *et al.*, Z. Phys. C **53**, 207 (1992).
[16] G.T. Jones *et al.*, Z. Phys. C **57**, 197 (1993).
[17] V. Jain *et al.*, Phys. Rev. D **41**, 2057 (1990).
[18] M. Aderholz *et al.*, Phys. Rev. D **45**, 2232 (1992).
[19] D. DeProspo, Ph.D. thesis, Rutgers University, 1991.
[20] Particle Data Group, K. Hikasa *et al.*, Phys. Rev. D **45**, S1 (1992).
[21] H.G. Heilmann, Bonn Internal Report No. WA21-int 1, 1978 (unpublished).
[22] P. Abreu *et al.*, Phys. Lett. B **275**, 231 (1992).
[23] P. Abreu *et al.*, Phys. Lett. B **318**, 249 (1993).
[24] D.H. Brick *et al.*, Phys. Rev. D **45**, 734 (1992).
[25] I. Bigi, Nuovo Cimento **41A**, 581 (1977).
[26] G.T. Jones *et al.*, Z. Phys. C **28**, 23 (1985).